Journal of Alloys and Compounds 503 (2010) L21–L25

Contents lists available at ScienceDirect

Journal of Alloys and Compounds

journal homepage: www.elsevier.com/locate/jallcom

Letter

Hydrothermal synthesis of novel Zn_2SnO_4 octahedron microstructures assembled with hexagon nanoplates

Xiaoxu Ji, Xintang Huang*, Jinping Liu, Jian Jiang, Xin Li, Ruimin Ding, Yingying Hu, Fei Wu, Qiang Li

Center for Nanoscience and Nanotechnology, Department of Physics, Central China Normal University, Wuhan 430079, Hubei, PR China

ARTICLE INFO

Article history:
Received 13 October 2009
Received in revised form 4 December 2009
Accepted 6 December 2009
Available online 20 June 2010

Keywords:
Semiconductors
Crystal growth
Optical properties

ABSTRACT

Zn_2SnO_4 with novel octahedron structures have been successfully synthesized on a large scale by applying surfactant hexadecyl trimethyl ammonium bromide (CTAB) throughout controllable hydrothermal reaction. X-ray diffraction (XRD), scanning electron microcopy (SEM), transmission electron microscopy (TEM), and high-resolution transmission electron microscopy (HRTEM) were used to characterize the final products. The results have revealed that three-dimensional (3D) Zn_2SnO_4 octahedrons were assembled with numerous intercrossed hexagon nanoplates with a mean edge length of 300 nm and an average thickness of 50 nm. Based on the time-dependent experimental results, the growth mechanism has been thoroughly investigated. The morphology of as-prepared octahedrons evolved from cubes with branched structures on their surfaces to octahedrons assembled with hexagon nanoplates, indicating that the process of crystal growth was controlled by a crystallization–dissolution–recrystallization growth mechanism. More importantly, we found that CTAB played a key role during the total formation process of as-obtained Zn_2SnO_4 octahedrons. UV–vis spectroscopy was further employed to estimate the band gap energy of the octahedron microstructures.

1. Introduction

It is well known that there is a strong correlation between the chemicophysical properties and the shape, size, and structure of materials. As a result, design and synthesis of novel nano- and microstructured materials have been intensively attracted not only for their significance in basic scientific research but also for various potential applications in fields such as catalysis, biological labeling, sensor and hydrogen storage [1–4]. In particular, three-dimensional (3D) nano- and microstructures with well controlled morphology and architecture have been a hot research topic in recent years [5,6]. Hydrothermal synthesis, as a well-known traditional wet chemical process, is a promising method for direct preparation of advanced nanostructures because of its advantages such as operational simplicity, cost-efficiency, and the capability for large-scale production. In terms of the reaction, the chemicophysical parameters of the system, such as temperature, reaction duration time, concentration of alkaline, and surfactants can be varied easily to control the kinetics and thermodynamics in the nucleation and growth of nanocrystals [7]. Recently, this facile wet chemical route has been widely employed to prepare various novel nanostructures.

As an important semiconductor material with a typical inverse spinel structure and a band gap of 3.6 eV, Zn_2SnO_4 (ZTO) has gained much more attention. ZTO has promising applications in photovoltaic devices, combustible gases and humidity detection, photo-electrochemistry, functional coatings, and transparent conducting electrodes owing to its good electron mobility, high-electrical conductivity, and low visible absorption [8–13]. Recently, such potential applications as electrode material for Li-ion batteries and dye-sensitized solar cells (DSSCs) have been demonstrated [12,14–16]. In the literatures, ZTO has been prepared via thermal evaporation [7], high-temperature calcinations [17,18], sol–gel synthesis [10], ball-milling [19], chemical vapor deposition [20], radio frequency magnetron sputtering [13,21], hydrothermal reaction [12,22–24] and thermal plasma [25]. However, it is difficult to obtain a single phase of ZTO by conventional solid-state reaction. Aimed to gain pure, uniform, and well-crystallized products, hydrothermal method is considered to be a feasible method to synthesize ZTO materials compared to traditional ways. Fang et al. [22] synthesized ZTO under hydrothermal conditions for the first time, who reported several experimental parameters for the effect of phase formation. Recently, ZTO was synthesized by the reaction of inorganic salt with concentrated aqueous sodium hydroxide, ammonia, or hydrazine hydrate solution under hydrothermal conditions, obtaining cube-shaped, spherical, rodlike ZTO nanocrystals [14,15,23,26]. To the best of our knowledge, no reports on the preparation of hierarchically microstructured ZTO octahedron assembled by nanoplates via a facile hydrothermal route have been

* Corresponding author. Fax: +86 27 67861185.
E-mail address: xthuang@phy.ccnu.edu.cn (X. Huang).

0925-8388/$ – see front matter © 2009 Elsevier B.V. All rights reserved.
doi:10.1016/j.jallcom.2009.12.038

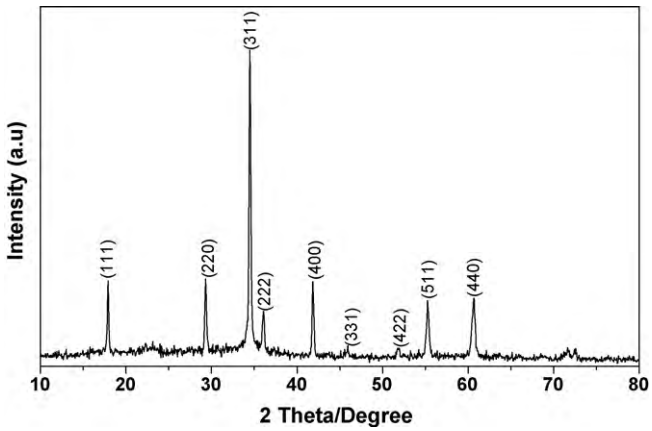

Fig. 1. XRD result of the as-obtained octahedron microstructures assembled with hexagon nanoplates.

published. In this study, we report for the first time the hydrothermal synthesis of ZTO with uniform hierarchical microstructures at 200 °C in the presence of hexadecyl trimethyl ammonium bromide (CTAB). The as-grown octahedrons were comprised of numerous intercrossed hexagon nanoplates with a mean edge length of 300 nm and a mean thickness of 50 nm. It is noticeable that the capping ligand CTAB is a crucial factor to shape octahedrons ZTO. No octahedron structures can be obtained in the absence of CTAB. Furthermore, the band gap energy of the microstructure is determined to be 3.6 eV by optical absorption.

2. Experimental

2.1. Preparation of octahedron Zn_2SnO_4

All the chemicals are of analytical grade without further treatments. In a typical procedure, CTAB (0.16 g), $SnCl_4{\cdot}5H_2O$ (0.025 M) and $ZnSO_4{\cdot}7H_2O$ (0.05 M) were dissolved with distilled water respectively, and then the obtained solutions were adequately mixed together. Acting as a mineralizer, NaOH solution (1 M) was dropped to the above solution to form a white precipitation mixture. After a few minutes of magnetic stirring, the mixture was transferred into a Teflon-lined stainless-steel autoclave (100 ml), kept at a temperature of 200 °C in an electric oven for different time, and allowed to cool to room temperature naturally. The product was collected, washed with several times by absolute alcohol

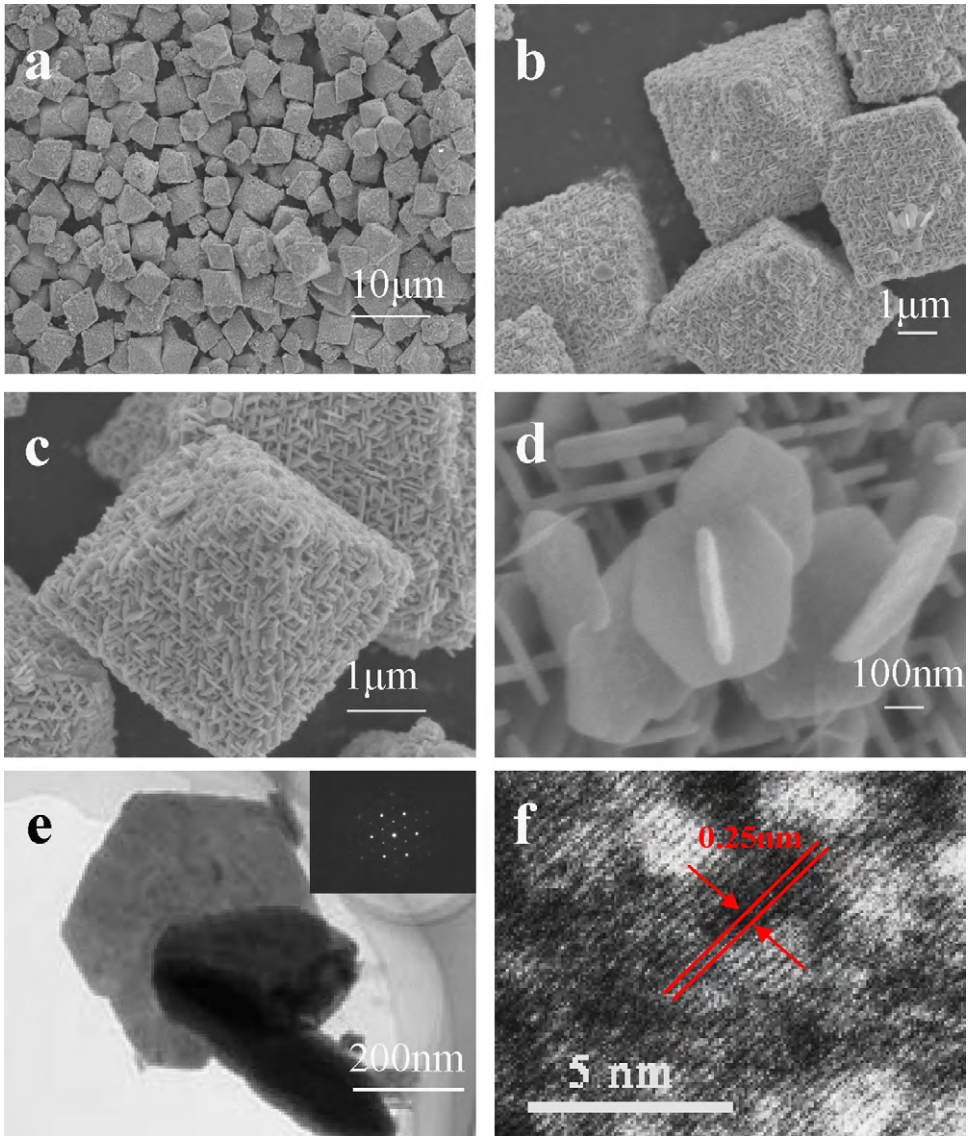

Fig. 2. (a) Low-magnification and (b) high-magnification SEM images of the as-obtained hierarchical octahedron microstructures. (c) SEM image of single octahedron. (d) SEM image of several nanoplates. (e) TEM image and the corresponding SAED of nanoplates assembled with octahedron. (f) HTEM image of the nanoplate.

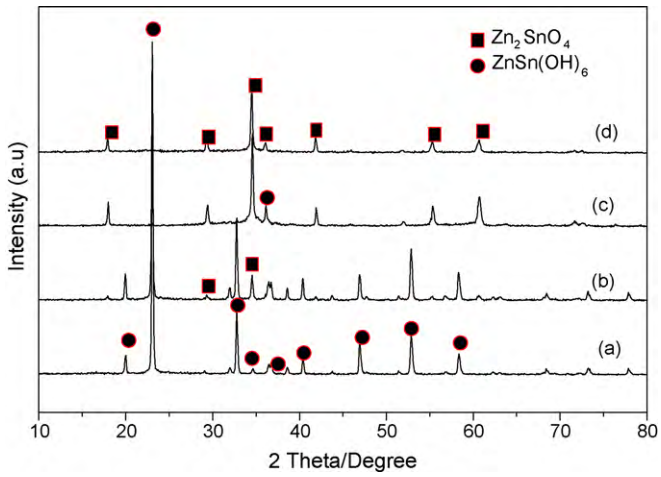

Fig. 3. XRD results of as-obtained products at different reaction time of (a) 2 h, (b) 4 h, (c) 6 h, and (d) 20 h.

and distilled water, and finally dried in a vacuum at 60 °C for 5 h before the further characterizations. To investigate the intermediates of the octahedron Zn_2SnO_4, the synthesis was stopped at different stages during the total synthesis process.

2.2. Sample characterizations

The morphology of the as-prepared product was characterized by field-emission scanning electron microscopy (FESEM, JEOL, JSM-6700F). The crystalline structure of the product was analyzed by an X-ray diffractometer (XRD, Y-2000) with Cu Kα radiation (λ = 1.5418 Å) at a scan rate of 0.04° s^{-1}. Transmission electron microscopy (TEM) and high-resolution transmission electron microscopy (HRTEM) observations were carried out on a JEOL JEM-2010 instrument in bright field. Room-temperature UV–vis absorption spectrum was recorded on a UV-2550 spectrophotometer in the wavelength range of 300–800 nm.

3. Results and discussion

3.1. Characterization of Zn_2SnO_4 octahedron microstructures

XRD pattern of the as-obtained octahedron Zn_2SnO_4 is shown in Fig. 1. All diffraction peaks are consistent with the JCPDS (74-2184) data of the pure spinel Zn_2SnO_4 with a lattice parameter of 0.8650 nm. The peaks correspond to an inverse spinel structure, where all Sn^{4+} atoms are octahedrally coordinated, while half of the Zn^{2+} atoms are distributed in tetrahedral coordination and the other half in octahedral coordination [27]. No peaks originating from impurities are observed.

SEM and TEM were employed in the characterization of ZTO. Fig. 2a is the low-magnification SEM image of the as-obtained product, indicating a high yield of these microstructures. As can be seen in Fig. 2b, a number of octahedrons with an average diameter of 2–4 μm are clearly observed. From Fig. 2c, a detailed observation of a single octahedron shows that these octahedrons are composed of numerous nanoplates. It is noteworthy that these nanoplates almost vertically stand on the octahedron's surface and alternately connect with each other to form networks. As displayed in Fig. 3d, the nanoplates which have a mean edge length of 300 nm and a mean thickness of 50 nm are densely interconnected. Fig. 3e shows typical TEM image of several nanoplates from the octahedron and the inset manifests the SAED pattern, which exhibits a regular and clear hexagon spot array, indicating high single-crystalline quality of as-prepared ZTO. From HRTEM image in Fig. 3f, the lattice interplanar spacing is measured to be about 0.25 nm, corresponding to the (2 2 2) plane of the microstructure in the XRD result.

3.2. Growth mechanism

To investigate the growth mechanism of such octahedron microstructure, several experiments at different reaction time were carried out. Through the time-dependent experiments, we could clearly observe the evolution of structure and morphology of ZTO.

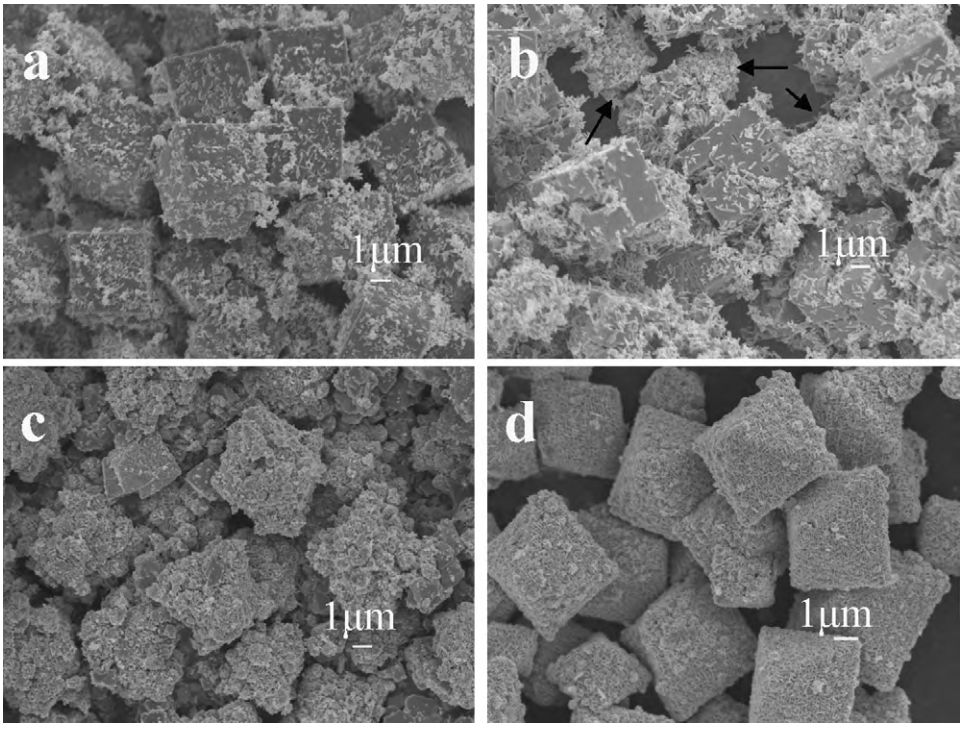

Fig. 4. SEM images of as-obtained products at different reaction time of (a) 2 h, (b) 4 h, (c) 6 h and (d) 20 h.

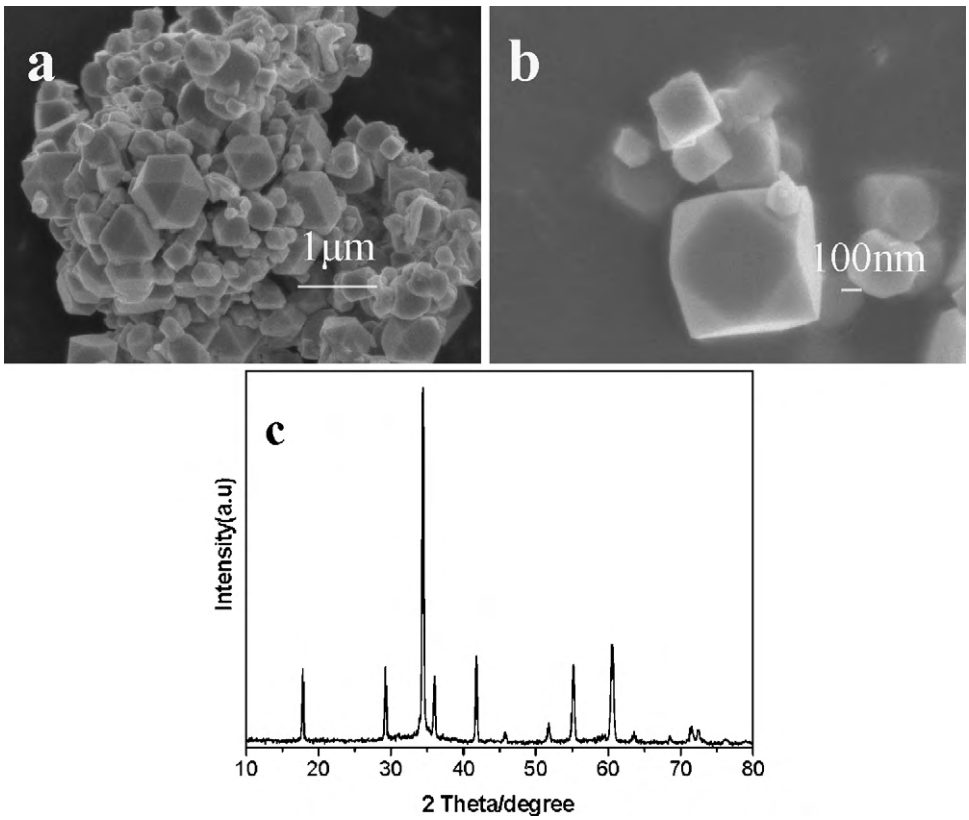

Fig. 5. (a) Low-magnification and (b) high-magnification SEM images. (c) XRD result of the product obtained in the absence of CTAB.

Fig. 3 shows the XRD patterns of the as-obtained samples within different reaction time. Undergoing a hydrothermal treatment for a short while, $ZnSn(OH)_6$ phase coexists with ZTO phase. When the reaction time sustains 2 h, only $ZnSn(OH)_6$ phase could be shown in the XRD pattern. After 4 h, the $ZnSn(OH)_6$ diminishes gradually compared to the samples with the reaction time of 2 h, and some weak diffraction peaks of ZTO appear. When the reaction time increased to 6 h or even longer, all the peaks of ZTO could be obviously observed. It is obvious that the intensity of ZTO peaks increased with reaction time. After 20 h, we find that the products completely evolve from $ZnSn(OH)_6$ to ZTO phase. The results of XRD patterns with different reaction time display the crystallization state of the prepared products. It would assist us to observe the growing process of the ZTO.

To understand how the ZTO hierarchical microstructures are formed, the time-dependent morphological evolution process has been examined by SEM. Representative SEM images of different reaction time are shown in Fig. 4. After reaction for 1 h, many cubes with rough surface are observed, as shown in Fig. 4a. We can see some protuberances on the surface of the cubes. With the reaction time up to 4 h, we can find some octahedrons assembled with nanoplates and nanoparticles (black arrow) besides cubes with protuberances (Fig. 4b). As the reaction time increases to 6 h, all cubic $ZnSn(OH)_6$ turns into octahedral ZTO, which is assembled with nanoplates and nanoparticles (Fig. 4c). When the reaction time is up to 20 h, a significant change could be observed in the morphology of the ZTO microstructures. The products have evolved from cubes with rough surfaces into a complex micro/nanoarchitecture. We obtained uniform and pure octahedron with delicate surface structure (Fig. 4d). On the basis of the time-dependent experiments, it has been suggested that the formation of octahedron ZTO microstructures may result from the crystal growth mechanism "crystallization–dissolution–recrystallization". Under the hydrothermal reactions, $ZnSn(OH)_6$ nuclei quickly formed in the

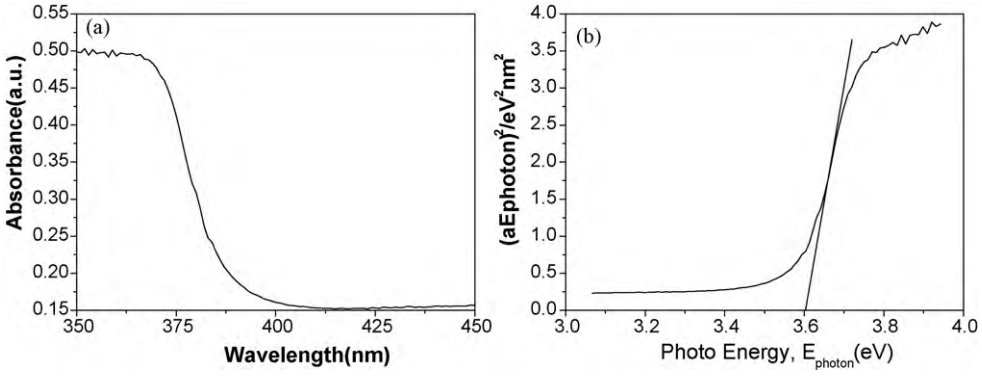

Fig. 6. (a) UV–vis diffuse reflectance spectra and (b) $(\alpha E_{photon})^2 \sim E_{photon}$ curve of the octahedron ZTO in the presence of CTAB.

solution, and hereafter the growth of the nuclei into cube-shaped crystals went on. Then, secondary nucleation occurred on the edge and surfaces of these cube-shaped crystals. The rough surface of the obtained $ZnSn(OH)_6$ cubes at the beginning of reactions is considered to be ascribed to the gradually dissolution of the cube crystals because of the large solubility and metastability of $ZnSn(OH)_6$ compared to ZTO. The metastable intermediate phase decomposed and recrystallized to form ZTO nuclei according to the "dissolution–recrystalline" mechanism.

We further emphasize the importance of CTAB in the formation of the novel octahedron ZTO microstructures. As shown in Fig. 5a, without CTAB we cannot obtain any octahedron ZTO micro/nanoarchitectures except for some bulk micro-particles. The XRD result of the product obtained in the absence of CTAB is displayed in Fig. 5c, from which a pure spinel ZTO can be identified. The experimental result has indicated that CTAB has played an important role in the process of assembling octahedron ZTO microstructures and further research works would be done to investigate the CTAB's function in detail.

Diffuse reflectance spectroscopy is a useful tool to reveal the energy structures and optical properties of semiconductor nanocrystal, and the migration of the light-induced electrons and holes are the key factors to control photocatalytic reaction, which is related to the electronic structure characteristics of the materials [28]. Fig. 6a shows the UV–visible diffuse reflectance spectrum of as-prepared Zn_2SnO_4 powders. It can be seen that the octahedron Zn_2SnO_4 microstructure has a steep absorption edge in visible range, indicating that the absorption relevant to the band gap is due to the intrinsic transition of the semiconductors rather than the transition from impurity levels. According to the equation $\alpha E_{photon} = A(E_{photon} - E_g)^{1/2}$ (where α, E_{photon}, and E_g are the absorption coefficient, the discrete photon energy, and the bandgap energy, respectively; A is a constant) [29], a classical Tauc approach is further employed to estimate the E_g of octahedron Zn_2SnO_4 microstructures. The plot of $(\alpha E_{photon})^2 \sim E_{photon}$ based on the direct transition is shown in Fig. 6b. The extrapolated value (the straight line to the X-axis) of E_{photon} at $\alpha = 0$ gives an absorption edge energy corresponding to $E_g = 3.6$ eV. This value accords with the value of bulk Zn_2SnO_4 (3.6 eV).

4. Conclusions

In summary, novel Zn_2SnO_4 octahedrons assembled with hexagon nanoplates have been successfully synthesized by means of hydrothermal method with the help of surfactant CTAB for the first time. Our experimental results indicate that the formation of octahedron microstructures is dominated by a crystallization–dissolution–recrystallization growth mechanism. CTAB plays important roles in the formation of well-defined microstructures. The experimental results suggest that three different growth stages are involved: (i) generation of primary metastable intermediate phase cube-shaped $ZnSn(OH)_6$; (ii) the dissolution of cube-shaped $ZnSn(OH)_6$ and formation of Zn_2SnO_4 nuclei; (iii) self-assembling Zn_2SnO_4 octahedron microstructures composed of hexagon nanoplates. This method presents a way for the controlled synthesis of multicomponent metal oxides.

Acknowledgment

The authors gratefully acknowledge the financial support from the National Natural Science Foundation of China (No. 50872039).

References

[1] W. Li, H. Cheng, J. Alloys Compd. 448 (2008) 287–292.
[2] J. Wang, G.D. Liu, Y.H. Lin, Small 2 (2006) 1134–1138.
[3] Q. Cao, J.A. Rogers, Adv. Mater. 21 (2009) 29–53.
[4] S. Ma, M.X. Gao, R. Li, H.G. Pan, Y.Q. Lei, J. Alloys Compd. 457 (2008) 457–464.
[5] G.Z. Shen, Y. Bando, J.Q. Hu, D. Golberg, Appl. Phys. Lett. 90 (2007) 123101.
[6] G.Z. Shen, Y. Bando, D. Golberg, Appl. Phys. Lett. 88 (2006) 123107.
[7] J.S. Jie, G.Z. Wang, X.H. Han, J.P. Fang, Q.X. Yu, Y. Liao, B. Xu, Q.T. Wang, J.G. Hou, J. Phys. Chem. B 108 (2004) 8249–8253.
[8] P. Gorrn, P. Holzer, T. Riedl, W. Kowalsky, J. Wang, T. Weimann, P. Hinze, S. Kip, Appl. Phys. Lett. 90 (2007) 063502.
[9] S. Dutta, A. Dodabalapur, Sens. Actuators B: Chem. 143 (2009) 50–55.
[10] G. Fu, H. Chen, Z.X. Chen, J.X. Zhang, H. Kohler, Sens. Actuators B: Chem. 81 (2002) 308–312.
[11] C.W. Yang, H.Y. Yeom, D.C. Paine, Thin Solid Films 516 (2008) 3105–3111.
[12] X.J. Zhu, L.M. Geng, F.Q. Zhang, Y.X. Liu, L.B. Cheng, J. Power Sources 189 (2009) 828–831.
[13] Y.S. Stato, J. Kiyohara, A. Hasegawa, T. Hattori, M. Ishida, N. Hamada, N. Oka, Y. Shigesato, Thin Solid Films 518 (2009) 1304–1308.
[14] A. Rong, X.P. Gao, G.R. Li, T.Y. Yan, H.Y. Zhu, J.Q. Qu, D.Y. Song, J. Phys. Chem. B (2006) 14754–14760.
[15] B. Tan, E. Toman, Y. Li, Y. Wu, J. Am. Chem. Soc. 129 (2007) 4162–4163.
[16] M.A.A. Aviles, Y.Y. Wu, J. Am. Chem. Soc. 131 (2009) 3216–3224.
[17] C. Wang, X.M. Wang, J.C. Zhao, B.X. Mai, G.Y. Sheng, P.A. Peng, J.M. Fu, J. Mater. Sci. 37 (2002) 2989–2996.
[18] I. Stambolova, A. Toneva, V. Blaskov, D. Radev, Y. Tsvetanova, S. Vassilev, P. Peshev, J. Alloys Compd. 391 (2005) L1–L4.
[19] F. Belliard, P.A. Connor, J.T.S. Irvine, Solid States Ionics 135 (2000) 163–167.
[20] Q.R. Hu, P. Jiang, H. Xu, Y. Zhang, S.L. Wang, X. Jia, W.H. Tang, J. Alloys Compd. 484 (2009) 25–27.
[21] M.V. Nikolić, K. Satoh, T. Ivetić, K.M. Paraskevopoulos, T.T. Zorba, V. Blagojević, L. Mančić, P.M. Nikolić, Thin Solid Films 516 (2008) 6293–6299.
[22] J. Fang, A.H. Huang, P.X. Zhu, N.S. Xu, J.Q. Xie, J.S. Chi, S.H. Feng, R.R. Xu, M.M. Wu, Mater. Res. Bull. 36 (2001) 1391–1397.
[23] H.L. Zhu, D.R. Yang, G.X. Yu, H. Zhang, D.L. Jin, K.H. Yao, J. Phys. Chem. B 110 (2006) 7631–7634.
[24] X.L. Fu, X.X. Wang, J.L. Long, Z.X. Ding, T.J. Yan, G.Y. Zhang, Z.Z. Zhang, H.X. Lin, X.Z. Fu, J. Solid State Chem. 182 (2009) 517–524.
[25] H.F. Lin, S.C. Liao, S.W. Huang, C.T. Hu, Mater. Chem. Phys. 117 (2009) 9–13.
[26] T.L. Villarreal, G. Boschloo, A. Hagfeldt, J. Phys. Chem. C 111 (2007) 5549–5556.
[27] D.L. Young, D.L. Williamson, T.J. Coutts, J. Appl. Phys. 91 (2002) 1464–1472.
[28] A. Kudo, I. Tsuji, H. Kato, Chem. Commun. (2002) 1958–1959.
[29] S. Tsunekawa, T. Fukuda, A. Kasuya, J. Appl. Phys. 87 (2000) 1318–1321.